COMPLEX SYSTEM MODELING AND SIMULATION
ISSN 2096-9929 05/06 pp 67–81
Volume 4, Number 1, March 2024
DOI: 10.23919/CSMS.2024.0002

Estimation-Correction Modeling and Chaos Control of Fractional-Order Memristor Load Buck-Boost Converter

Lin Wang, Cong Wang*, Hongli Zhang*, Ping Ma, and Shaohua Zhang

Abstract: A fractional-order memristor load Buck-Boost converter causes periodic system oscillation, electromagnetic noise, and other phenomena due to the frequent switching of the switch in actual operation, which is detrimental to the stable operation of the power electronic converter. It is of great significance to the study of the modeling method and chaos control strategy to suppress the nonlinear behavior of the Buck-Boost converter and expand the safe and stable operation range of the power system. An estimation-correction modeling method based on a fractional active voltage-controlled memristor load peak current Buck-Boost converter is proposed. The discrete numerical solution of the state variables in the continuous mode of the inductor current is derived. The bursting oscillation phenomenon when the system introduces external excitation is analyzed. Using bifurcation, Lyapunov exponent, and phase diagrams, a large number of numerical simulations are performed. The results show that the Buck-Boost converter is chaotic for certain selected parameters, which is the prerequisite for the introduction of the controller. Based on the idea of parameter perturbation and state association, a three-dimensional hybrid control strategy for a fractional memristor Buck-Boost converter is designed. The effectiveness of the control strategy is verified by simulations, and it is confirmed that the system is controlled in a stable periodic state when the external tunable parameter s, which represents the coupling strength between the state variables in the system, gradually decreases in [–0.4, 0]. Compared with integer-order controlled systems, the stable operating range of fractional-order controlled systems is much larger.

Key words: fractional-order memristor Buck-Boost converter; estimation-correction algorithm; hybrid control strategy; bursting oscillation

1 Introduction

Buck-Boost converters, as crucial research subjects in integrated power electronics, have propelled the rapid progress of electronic products and are widely used in industrial and commercial sectors, such as electric vehicles[1], portable electronic devices[2], and photovoltaic power generation systems[3, 4]. However, the Buck-Boost converter exhibits strong nonlinear characteristics, including period-double bifurcation, boundary collision bifurcation, and chaos[5], which directly impact the stable operation and safe and reliable performance of the converter system. Currently, by conducting research on various DC-DC converters from different perspectives[6, 7], productive research results and a series of effective control methods have been achieved[8–10]. Zheng and Peng[11] employed passive delay feedback and improved sliding mode control methods for a voltage control Buck-Boost converter operating in chaotic bifurcation and

• Lin Wang, Cong Wang, Hongli Zhang, Ping Ma, and Shaohua Zhang are with the School of Electrical Engineering, Xinjiang University, Urumqi 830017, China. E-mail: 13565985491@163.com; wangc@xju.edu.cn; zhlxju@163.com; 694073078@qq.com; 510488900@qq.com.
* To whom correspondence should be addressed.
※ This article was recommended by Associate Editor Rebing Wu.
Manuscript received: 2023-12-08; revised: 2024-01-18; accepted: 2024-03-15

intermittent modes to achieve the stable operation of the control system under a single-cycle condition. Wang et al.[12] utilized the perturbation of resonance parameters to control the chaos of bidirectional DC-DC converters, improving their stability in DC microgrids. Zhang et al.[13] proposed and verified a fault-tolerant sampling data controller suitable for a Buck converter that resolved the issue of power system instability.

Due to their nonlinearity, plasticity, and nonvolatile nature, memristors have been used to develop various chaotic oscillation circuits[14], and neuromorphic computing circuits[15] have been developed in recent years. Additionally, incorporating a memristor load into a Buck-Boost converter allows for no alteration of the bifurcation-to-chaos path, the shifting of the bifurcation point forward, a narrower stable operating range, and an improved nonlinear response. Bao et al.[16] proposed a peak current mode memory Buck converter and investigated the dynamic characteristics of a peak current mode (PCM) memory Buck-Boost converter, revealing the dynamic influence of the memory load on the Buck-Boost converter. Currently, research on combining memristors and DC-DC converters has extended from integers to fractional orders. Wu et al.[17] simulated the dynamics of a fractional memristor Boost converter operating in the inductor current discontinuous mode and discovered that the fractional-order and memory load circuit system could expend the stable working range of the Boost converter. Zhang et al.[9] used time-delayed feedback control to suppress the bifurcation and chaotic behavior of Boost converters in PCM with memristor loads and verified the effectiveness of the control. Yang et al.[18] suppressed the chaos by applying a small disturbance to the peak current of a switched-inductor Buck-Boost (SIBB) converter with a memristor, ensuring the normal operation of the converter.

Fractional-order physical models offer a more accurate representation of the physical properties of nonlinear systems compared to integer-order physical models[19, 20]. Therefore, studying the mathematical modeling of fractional-order memristor load Buck-Boost converters is essential in promoting the application and extension of fractional-order theory in DC-DC converters. The numerical simulation method and analytical modeling method commonly used analytical approaches for nonlinear systems[21, 22]. Yang et al.[23] studied a non-integer order flyback converter, modeled the state space, and analyzed the converter for AC/DC, showing that non-integer orders had a smaller overshoot compared to first-order systems. The Bogacki-Shampine method and the estimation-correction method[24] are classical algorithms in numerical simulation algorithms that solve state variables based on the characteristics of circuit components. Among these algorithms, the estimation-correction algorithm[25] is a powerful numerical tool for studying the nonlinear dynamic behavior of a converter by approximating the exact solution of non-integer order transformer state variables in the time domain.

Nonlinear phenomena such as bifurcation and chaos cause periodic oscillation, electromagnetic interference, sudden system failure, and other phenomena that impede the stable operation of power electronic systems. Consequently, the proficient control strategy of fractional-order converters commands substantial scholarly attention. Fractional calculus is a promising tool for improving the accuracy of physical models and controlling the dynamic behavior of nonlinear systems closer to real-world values[26]. Xie et al.[27] proposed a new adaptive sliding mode controller that combined fractional calculus and synchronous control to enable robustness, a small steady-state error, and a fast response in a Buck-Boost converter. Mohadeszadeh et al.[28] developed a fractional reset controller for disturbance elimination and stable system output in fractional Buck converter simulations, proving the applicability and effectiveness of the controller.

The literature analysis indicates that recent years have seen in-depth research on modeling and analyzing memory load converters. However, there is a lack of research on dynamic analysis and control strategy design based on fractional-order estimation-correction modeling methods. Thus, this paper proposes a hybrid control strategy based on the mathematical model constructed through the estimation-correction algorithm. This strategy effectively suppresses the chaos phenomenon of the Buck-Boost second-order current feedback converter with a fractional memristor load in the stable cycle operating condition by combining state correlation and parameter perturbation.

The main contributions of this study can be summarized as follows:

(1) The estimation-correction method accurately discretizes and numerically solves the three-dimensional differential equation system of a

fractional-order memristor converter, allowing for the accurate modeling and direct calculation of the converter's inductor current, capacitor voltage, and memristor capacitor voltage.

(2) A hybrid control strategy is implemented to couple control state variables by adjusting the externally adjustable parameter s. Additionally, the resulting bifurcation diagram of the converter output voltage, the phase diagram of the inductor current and capacitor voltage, and the time domain waveform of each state variable are analyzed to confirm the effectiveness of the designed three-dimensional non-integer order controller.

2 Fractional-Order Definition

The ${}_mD_t^\alpha$ calculus fractions are defined as[29]

$$ {}_mD_t^\alpha = \begin{cases} \dfrac{\mathrm{d}^\alpha}{\mathrm{d}t^\alpha}, & \alpha > 0; \\ 1, & \alpha = 0; \\ \displaystyle\int_m^t (\mathrm{d}\tau)^{-\alpha}, & \alpha < 0 \end{cases} \tag{1} $$

where α is the fractional-order, and t and m are the upper and lower limits, respectively.

Caputo fractional-order definition:

$$ {}_m^C D_t^\alpha f(t) = \frac{1}{\Gamma(n-\alpha)} \int_m^t \frac{f^{(n)}(\tau)}{(t-\tau)^{\alpha-n+1}} \mathrm{d}\tau, \quad 0 \leqslant n-1 < \alpha \leqslant n \tag{2} $$

where n is the smallest integer greater than order α, and $\Gamma(\cdot)$ is gamma function, expressed as follows:

$$ \Gamma(x) = \int_0^\infty t^{x-1} \mathrm{e}^{-t} \mathrm{d}t \tag{3} $$

where e^{-t} is the exponential function for time t.

The Laplace transform of the Caputo differential operator of order α is

$$ L\left\{ {}_m^C D_t^\alpha f(t) \right\} = s^\alpha F(s) - \sum_{k=0}^{n-1} s^k \left[\frac{\mathrm{d}^{\alpha-1-k} f(t)}{\mathrm{d}t^{\alpha-1-k}} \right]_{t=0}, \quad n-1 < \alpha \leqslant n \tag{4} $$

When the initial value of the system is set to zero, the Laplace transform expression for the fractional derivative is simplified to

$$ L\left\{ {}_m^C D_t^\alpha f(t) \right\} = s^\alpha F(s) \tag{5} $$

3 Estimation-Correction Modeling and Dynamic Analysis

3.1 Fractional-order memristor model

In this paper, an active voltage-controlled memristor is selected, as shown in Fig. 1. Figure 1a displays the equivalent circuit of the fractional-order memristor. Figure 1b displays the model. In Fig. 2, the resistor R in the Buck-Boost converter is replaced by the memristor circuit model in Fig. 1b[30].

A fractional unified mathematical model can be derived from the memristor circuit model:

$$ \begin{cases} \dfrac{\mathrm{d}^\gamma v_0}{\mathrm{d}t^\gamma} = \dfrac{V_m}{R_3 C_0^q} - \dfrac{v_0}{R_4 C_0^q}, \\ i_m = W(v_0) V_m = \dfrac{1}{R_8}\left(1 - \dfrac{R_7}{R_5} + \dfrac{R_7}{R_6} g v_0\right) V_m, \\ W(v_0) = \dfrac{i_m}{V_m} = \dfrac{1}{R_8}\left(1 - \dfrac{R_7}{R_5} + \dfrac{R_7}{R_6} g v_0\right) \end{cases} \tag{6} $$

Given a sinusoidal input voltage $V_m = A\sin(2\pi f)$, where A is the amplitude of the input voltage and f is the excitation frequency. If the excitation amplitude $A = 2$ V, excitation frequency $f = 51$ kHz, and order γ of 0.50, 0.85, 0.90, 0.96, and 1.00 are entered, the comparison $V_m - i_L$ curve of each order of the memristor is shown in Fig. 3a. Furthermore, the $V_m - i_L$ characteristic curve of the variable order memristor is a narrow hysteresis loop with an oblique "8" shape that

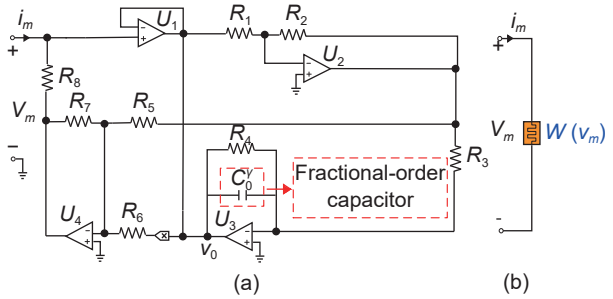

Fig. 1 Equivalent circuit of (a) a fractional-order memristor and (b) its model.

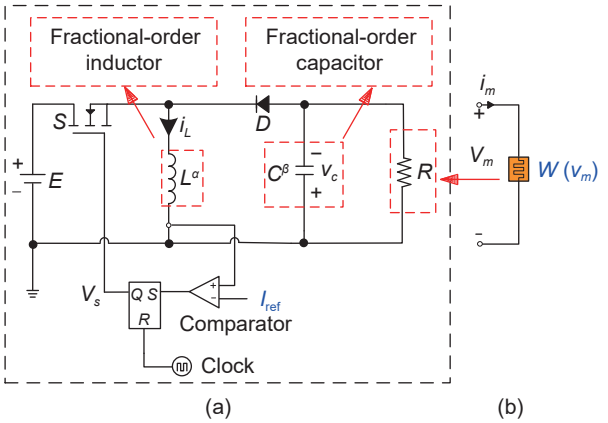

Fig. 2 Fractional-order peak current type memristor Buck-Boost converter schematic.

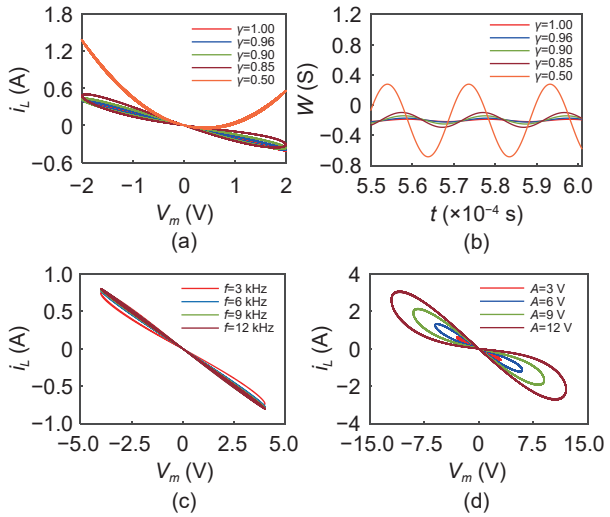

Fig. 3 Numerical simulation of a fractional-order memristor.

shrinks at the origin, and when the order of the system decreases, the area of the side lobe of the narrow hysteresis loop changes in negative correlation to the order and then gradually shrinks to a single-valued function. When $\gamma = 0.50$, the tight hysteresis loop changes from two and four quadrants to one and two quadrants, as shown in Fig. 3b. Hence, the memristor appears positive and passive. The size of the side lobe area can reflect the strength of the memrization of each array of memristors, which are positively correlated with each other.

Figure 3c shows the tight hysteresis loop at the system frequency at 3, 6, 9, and 12 kHz for a fixed system order of $\gamma = 0.85$ and an amplitude of $A = 2$ V. It can be observed that with the continuous increase of the system frequency f, the area of the side lobe of the narrow hysteresis loop gradually decreases and shrinks to a straight line at infinite frequency, which corresponds to the essential characteristics of memristors.

Figure 3d shows the shape of the narrow hysteresis loop at the system order $\gamma = 0.96$, excitation frequency $f = 51$ kHz, and system amplitude A at 3, 6, 9, and 12 V. It can be observed that the area of the tight hysteresis loop of the system is positively correlated with the change in the amplitude of the input voltage, but its oblique "8" shape does not change with the amplitude.

By numerically simulating the tight hysteresis loop of the memristor using MATLAB, it is proved that the fractional voltage-controlled memristor satisfies the essential characteristics of the memristor element.

3.2 Estimation-correction modeling of a fractional-order memristor Buck-Boost transformer

Figure 2 shows the system circuit diagram of the system in peak current mode. Figure 2a shows the Buck-Boost converter model. Figure 2b shows the memristor load model. The circuit model of the fractional-order memristor Buck-Boost converter is formed by replacing the pure resistance R in the Buck-Boost converter with the memristor load model $W(v_m)$ and expanding the capacitance and inductance in the circuit to the fractional-order based on the theory of fractional calculus.

The relationship between the fractional component voltage and current is defined as[31]

$$i(t) = C\frac{\mathrm{d}^{\beta}V(t)}{\mathrm{d}t^{\beta}} \tag{7}$$

$$V(t) = L\frac{\mathrm{d}^{\alpha}i(t)}{\mathrm{d}t^{\alpha}} \tag{8}$$

As shown in Fig. 4, the peak current I_{ref} is set, driven by the first clock cycle T. Switch Q is off, the diode is off, and the mode continues for time interval T_{on}, which is called State 1. When the inductor current $i_L \geqslant I_{\mathrm{ref}}$, the switch Q is turned off and the diode is on, and the mode continues at interval T_{off}, which is called State 2. Until the second clock goes up, the cycle ends, and the cycles continue in turn.

When the system is operating in continuous current mode:

Status 1: Switch Q is closed and diode D is off (T_{on})

$$\begin{cases} L\dfrac{\mathrm{d}^{\alpha}i_L}{\mathrm{d}t^{\alpha}} = E, \\ C\dfrac{\mathrm{d}^{\beta}v_c}{\mathrm{d}t^{\beta}} = \dfrac{1}{R_8}\left(1 - \dfrac{R_7}{R_5} + \dfrac{R_7}{R_6}gv_0\right)v_c, \\ C_0\dfrac{\mathrm{d}^{\gamma}v_0}{\mathrm{d}t^{\gamma}} = -\dfrac{v_c}{R_3} - \dfrac{v_0}{R_4} \end{cases} \tag{9}$$

Status 2: Switch Q is open and diode D is on (T_{off})

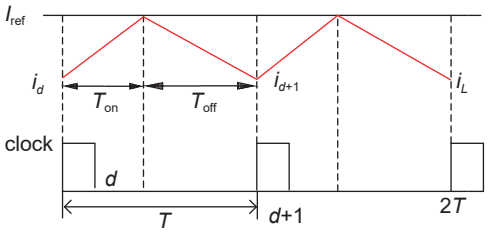

Fig. 4 Buck-Boost converter inductor current waveform in peak current mode.

$$\begin{cases} L\dfrac{\mathrm{d}^{\alpha}i_L}{\mathrm{d}t^{\alpha}} = -v_c, \\ C\dfrac{\mathrm{d}^{\beta}v_c}{\mathrm{d}t^{\beta}} = i_L + \dfrac{1}{R_8}\left(1-\dfrac{R_7}{R_5}+\dfrac{R_7}{R_6}gv_0\right)v_c, \\ C_0\dfrac{\mathrm{d}^{\gamma}v_0}{\mathrm{d}t^{\gamma}} = -\dfrac{v_c}{R_3}-\dfrac{v_0}{R_4} \end{cases} \tag{10}$$

Depending on the switching conditions of the converter, a unified mathematical model of the system can be created during the cycle:

$$\begin{cases} \dfrac{\mathrm{d}^{\alpha}i_L}{\mathrm{d}t^{\alpha}} = Q\dfrac{E}{L}-(1-Q)\dfrac{v_c}{L}, \\ \dfrac{\mathrm{d}^{\beta}v_c}{\mathrm{d}t^{\beta}} = (1-Q)\dfrac{i_L}{C}+\dfrac{1}{CR_8}\left(1-\dfrac{R_7}{R_5}+\dfrac{R_7}{R_6}gv_0\right)v_c, \\ \dfrac{\mathrm{d}^{\gamma}v_0}{\mathrm{d}t^{\gamma}} = -\dfrac{v_c}{C_0R_3}-\dfrac{v_0}{C_0R_4} \end{cases} \tag{11}$$

By combining the q-order differential equation $D_*^q y(x) = f(x, y(x))$ defined by Caputo with the initial condition $y^{(u)}(0) = y_0^{(u)}$, $u = 0, 1, ..., m-1$ and its discretization, a model for estimating and correcting the fractional calculus equation is obtained:

$$y_r(t_{d+1}) = \sum_{u=0}^{[q]-1}\frac{t_{d+1}^u}{u!}y_0^{(u)} + \frac{r^q}{\Gamma(q+2)}f\left(t_{d+1}, y_r^p(t_{d+1})\right) + \frac{r^q}{\Gamma(q+2)}\sum_{j=0}^{d}a_{j,d+1}f\left(t_j, y_r\left(t_j\right)\right) \tag{12}$$

The correction factor is given below:

$$a_{j,d+1} = \begin{cases} d^{q+1}-(d-q)(d+1)^q, j=0; \\ (d-j+2)^q+(d-j)^{q+1}-2(d-j+1)^{q+1}, \\ 1 \leqslant j \leqslant d; \\ 1, j = d+1 \end{cases} \tag{13}$$

where $m = [q]$ and $y_0^{(u)}$ are known initial values. The system parameters are set as indicated in Table 1.

The fractional-order estimation-correction model of the Buck-Boost converter with the memristor load at continuous conduction mode (CCM) with the switching period T can be obtained as follows:

Table 1 Time system parameter setting (t=t_{d+1}).

Parameter	Parameter value
Converter inductor current	$i_{Lr}(t_{d+1}) = i_{d+1}$
An approximate estimate of the initial value of the inductor current	$i^p{}_{Lr}(t_{d+1}) = i^p{}_{d+1}$
Converter capacitor voltage	$v_{cr}(t_{d+1}) = v_{c}{}_{d+1}$
An approximate estimate of the initial value of the capacitor voltage	$v^p{}_{cr}(t_{d+1}) = v_c{}^p_{d+1}$
Memristor capacitor voltage	$v_{0r}(t_{d+1}) = v_{0}{}_{d+1}$
An approximate estimate of the initial value of the capacitor voltage	$v^p{}_{0r}(t_{d+1}) = v_0{}^p_{d+1}$

$$\begin{cases} i_{d+1} = i_0 + \dfrac{r^{\alpha}}{\Gamma(\alpha+2)}\left(Q\dfrac{E}{L}-(1-Q)\dfrac{v_c{}^p_{d+1}}{L}\right)+ \\ \qquad \dfrac{r^{\alpha}}{\Gamma(\alpha+2)}\sum_{i=0}^{d}a_{i,d+1}^{\alpha}\left(Q\dfrac{E}{L}-(1-Q)\dfrac{v_c^i}{L}\right), \\ v_c^{d+1} = v_c^0 + \dfrac{r^{\beta}}{\Gamma(\beta+2)}\left((1-Q)\dfrac{i^p_{d+1}}{C}+\right. \\ \qquad \left.\dfrac{1}{CR_8}\left(1-\dfrac{R_7}{R_5}+\dfrac{R_7}{R_6}gv_0{}^p_{d+1}\right)v_c{}^p_{d+1}\right)+ \\ \qquad \dfrac{r^{\beta}}{\Gamma(\beta+2)}\sum_{i=0}^{d}a_{i,d+1}^{\beta}\left((1-Q)\dfrac{i_i}{C}+\right. \\ \qquad \left.\dfrac{1}{CR_8}\left(1-\dfrac{R_7}{R_5}+\dfrac{R_7}{R_6}gv_0^i\right)v_c^i\right), \\ v_0^{d+1} = v_0^0 + \dfrac{r^{\gamma}}{\Gamma(\gamma+2)}\left(-\dfrac{v_c{}^p_{d+1}}{C_0R_3}-\dfrac{v_0{}^p_{d+1}}{C_0R_4}\right)+ \\ \qquad \dfrac{r^{\gamma}}{\Gamma(\gamma+2)}\sum_{i=0}^{d}a_{i,d+1}^{\gamma}\left(-\dfrac{v_c^i}{C_0R_3}-\dfrac{v_0^i}{C_0R_4}\right) \end{cases} \tag{14}$$

where i_0, v_c^0, and v_0^0 are the initial values of the inductor current, capacitor voltage, and memristor capacitor voltage, respectively. $a_{i,d+1}^{\alpha}$, $a_{i,d+1}^{\beta}$, and $a_{i,d+1}^{\gamma}$ are the correction factors of the inductor current, capacitor voltage, and memristor capacitor voltage, respectively. i_{d+1}^p, $v_{c}{}^p_{d+1}$, and $v_0{}^p_{d+1}$ are approximate estimates of the initial values of the inductor current, capacitor voltage, and memristor capacitor voltage, respectively.

According to Eq. (13), the expression for the correction coefficient for each state variable in Eq. (14) can be written as

$$a_{i,d+1}^{\alpha} = \begin{cases} d^{\alpha+1}-(d-\alpha)(d+1)^{\alpha}, i=0; \\ (d-i+2)^{\alpha}+(d-i)^{\alpha+1}- \\ 2(d-i+1)^{\alpha+1},\ 1 \leqslant i \leqslant d; \\ 1, i = d+1; \end{cases}$$

$$a_{i,d+1}^{\beta} = \begin{cases} d^{\beta+1}-(d-\beta)(d+1)^{\beta}, i=0; \\ (d-i+2)^{\beta}+(d-i)^{\beta+1}- \\ 2(d-i+1)^{\beta+1},\ 1 \leqslant i \leqslant d; \\ 1, i = d+1; \end{cases} \tag{15}$$

$$a_{i,d+1}^{\gamma} = \begin{cases} d^{\gamma+1}-(d-\gamma)(d+1)^{\gamma}, i=0; \\ (d-i+2)^{\gamma}+(d-i)^{\gamma+1}- \\ 2(d-i+1)^{\gamma+1},\ 1 \leqslant i \leqslant d; \\ 1, i = d+1 \end{cases}$$

Approximate estimate of the initial value of the state variable is as follows:

$$y_r^p(t_{d+1}) = \sum_{u=0}^{[q]-1} \frac{t_{d+1}^u}{u!} y_0^{(u)} + \frac{1}{\Gamma(q)} \sum_{j=0}^{d} b_{j,d+1} f\left(t_j, y_r\left(t_j\right)\right) \tag{16}$$

where $b_{j,d+1} = \frac{t^q}{q}((d+1-j)^q - (d-j)^q)$ is the estimated coefficient.

From Eq. (16), the initial estimate of the stress can be derived as follows:

$$\begin{cases} i_{d+1}^p = i_0 + \dfrac{1}{\Gamma(\alpha)} \sum\limits_{i=0}^{d} b_{i,d+1}^{\alpha} \left(Q\dfrac{E}{L} - (1-Q)\dfrac{v_c^i}{L} \right), \\ v_{c_{d+1}^p} = v_c^0 + \dfrac{1}{\Gamma(\beta)} \sum\limits_{i=0}^{d} b_{i,d+1}^{\beta} \Bigg((1-Q)\dfrac{i_i}{C} + \\ \qquad \dfrac{1}{CR_8} \left(1 - \dfrac{R_7}{R_5} + \dfrac{R_7}{R_6} g v_0^i \right) v_c^i \Bigg), \\ v_{0_{d+1}^p} = v_0^0 + \dfrac{1}{\Gamma(\gamma)} b_{i,d+1}^{\gamma} \left(-\dfrac{v_c^i}{C_0 R_3} - \dfrac{v_0^i}{C_0 R_4} \right) \end{cases} \tag{17}$$

4 Dynamic Analysis of Fractional-Order Memristor Buck-Boost Converter

4.1 Bifurcation analysis

To study the dynamic characteristics of a fractional-order Buck-Boost converter with a memristor load before regulation, we select the 0.9-order that maximizes the fractional-order characteristics, while ensuring that the system operates in the inductor-current continuous mode. The following parameters are selected in Table 2.

The dimensionless treatment of Eqs. (9) and (10) is $x = i_L$, $y = v_c$, $z = v_0$, $t = R_8 C\tau$, $\tau_T = T(R_8 C)^{-1}$, $a = R_8 C L^{-1}$, $b = R_8$, $c = \frac{R_7}{R_6}$, $d = \frac{R_7}{R_5} - 1$, $m = \frac{R_8 C}{R_3 C_0}$, and $p = \frac{R_8 C}{R_4 C_0}$, where $V_m = -v_c$. From the component parameters in Table 2, the dimensionless parameter values can be calculated: $E = 2$ V, $a = b = c = g = 1$, $d = 0.2$, $m = 0.25$, and $p = 0.96$.

Table 2 System element parameters.

Parameter	Signification	Value
E	Input voltage	2 V
L	Inductance	0.05 mH
C	Capacitance	47 μF
I_{ref}	Reference current	5 A
g	Multiply gain	1
C_0	Memristor capacitors	10 nF
α,β,γ	System order	0.9 (adjustable)
R_1	Resistance	10 kΩ
R_2	Resistance	1 kΩ
R_3	Resistance	40 kΩ
R_4	Resistance	10 kΩ
R_5	Resistance	8.3 kΩ
R_6,R_7	Resistance	10 kΩ
R_8	Resistance	1 Ω

The available Status 1 is

$$\begin{cases} \dot{x} = aE, \\ \dot{y} = (cgx_3 - d)x_2, \\ \dot{z} = -mx_2 - px_3 \end{cases} \tag{18}$$

Status 2:

$$\begin{cases} \dot{x} = -ax_2, \\ \dot{y} = bx_1 + (cgx_3 - d)x_2, \\ \dot{z} = -mx_2 - px_3 \end{cases} \tag{19}$$

However, because the switch is constantly switched, the circuit may operate in a periodic state or a chaotic state.

For the selected parameters, Fig. 5 shows the bifurcation diagram of the capacitor voltage of the converter with the reference current, the three-dimensional phase diagram, and the Poincaré cross-sectional view. If the reference current of 5 A is chosen, the three-dimensional phase diagram is nested with infinite self-similar structures, and in the y-z plane of x=−5, it can be observed that the Poincaré cross-section diagram consists of innumerable points at this time.

Since the irregular change of the duty cycle D_c in each switching cycle causes the converter to become unstable and enter a chaotic state, it can better reflect the essential characteristics of the nonlinear phenomenon of the converter. Usually, when the voltage across the memristor load $W(v_0)$ consists of a chaotic signal and a periodic signal, the corresponding switching duty cycle consists of a chaotic signal and a periodic signal. When the reference currents I_{ref} are 5 A and 1 A, the duty cycle plots of the converter for each switching cycle are shown in Fig. 6. The unordered and equal duty cycles D_c in Fig. 6 further illustrate in fact that when I_{ref}= 5 A and 1 A, the transformer operates in chaotic and periodic states.

Therefore, it can be determined that when the selected parameter value and reference current in Table 2 are both 5 A, the system is in a chaotic state, and the chaos control is meaningful.

4.2 Bursting oscillation analysis

When the slow-changing parameter frequency in the Buck-Boost converter with memristor load is an order of magnitude different from the natural frequency of

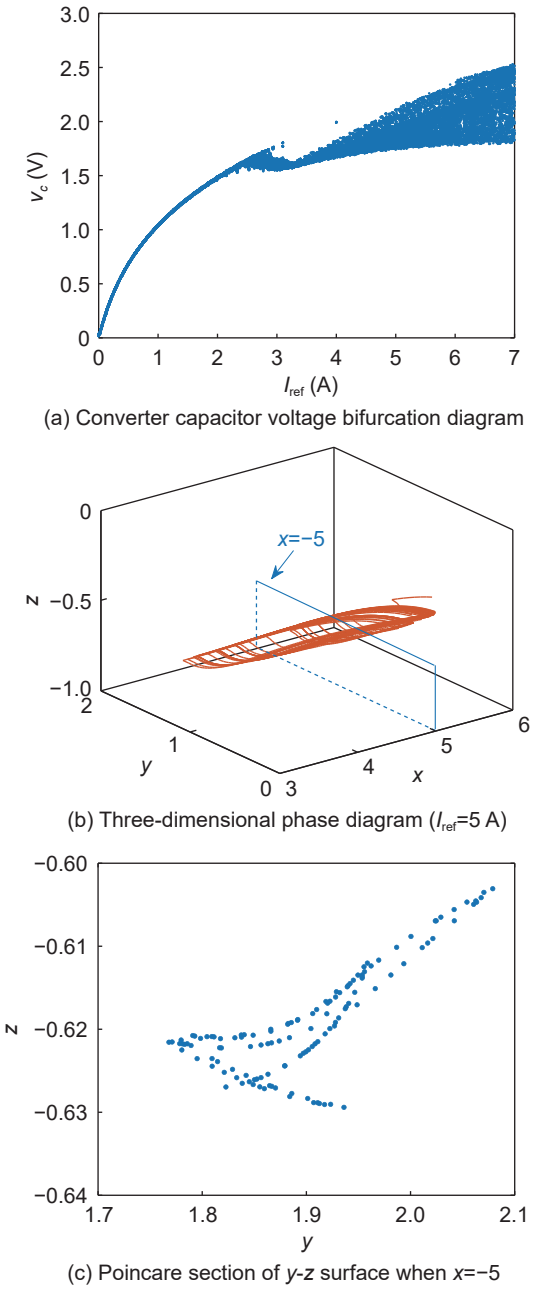

Fig. 5 Reference diagram of system chaos state selection.

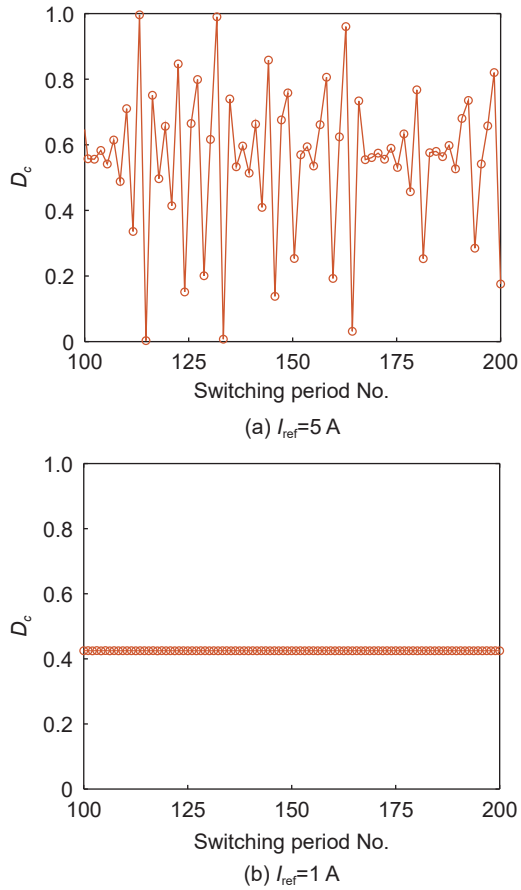

Fig. 6 System duty cycle D_c graph.

the system, the bursting oscillation behavior that is not conducive to the stable operation of the power system is generated. Introducing the external excitation into the equation of state of the transformer, the corresponding three-dimensional dynamic model is obtained as follows:

$$\begin{cases} \dot{x} = au_1 + \omega_1, \\ \dot{y} = u_2 x + (-d + cgz)y, \\ \dot{z} = -my\omega_2 - nz \end{cases} \tag{20}$$

The external periodic excitation $\omega_1 = A_1 \cos(\omega_1 t)$ is selected, the parameter excitation $\omega_2 = A_2 \cos(\omega_2 t)$ is the slow variable, A_i is the excitation amplitude, and ω_i is the excitation frequency, where i = 1, 2. When the value of (u_1, u_2) is $(E, 0)$, the system works in Status 1, as shown in Eq. (18), and when the value of (u_1, u_2) is $(-y, b)$, the system works in Status 2, as shown in Eq. (19). At $0 < \omega_i \leqslant 1$, the frequency of the system operating in external excitation Status 2 has an order of magnitude difference from the parameters in the reaction, resulting in a two-timescale coupling system.

The fixed parameters are a=1, b=1, c=1, d=0.03, m=0.25, n=0.96, ω_1=0.015, and ω_2=0.01. The initial value of the system is [0.1 0.1 0.1], the excitation amplitude A=0.1, and the periodic bursting oscillation mode and dynamic behavior evolution law of the fast on-cell system (Eq. (20)) are analyzed.

As shown in Fig. 7, the three-dimensional phase diagram and (y, z) planar phase diagram of a Buck-Boost converter with the memristor load are shown. It can be seen from Fig. 7 that when the converter works in the cluster oscillation mode of the excited state, the three state variables of the system are unstable, causing the system to switch back and forth between the three vortex oscillating attractor SPs. The process of

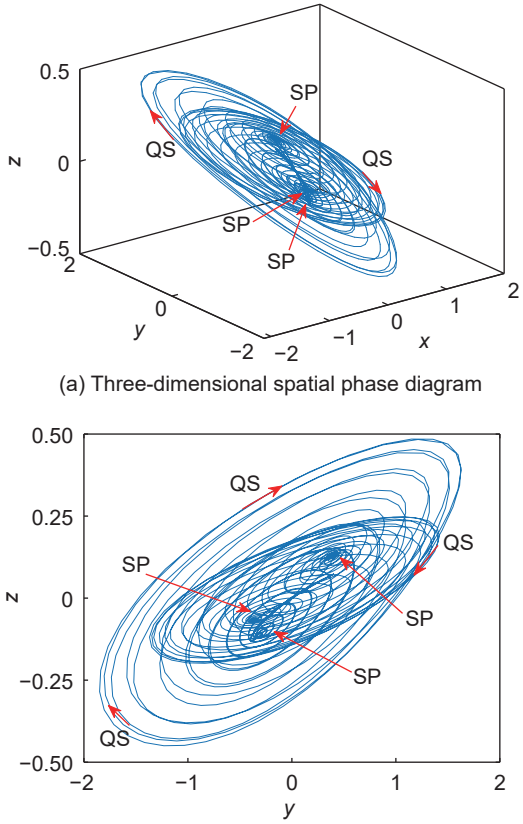

Fig. 7 Bursting oscillation attractors.

switching a state variable from a silent state to an excited state is represented as SP, and the transition process from one excited state to another is denoted as QS.

Figure 8 shows the time series of the state variables in the system. The timing diagram of the three state variables of the system (Eq. (20)) is shown in Fig. 8a, and the whole system has typical bursting oscillation behavior. As shown in Fig. 8b, based on the time series diagram of the system state variable z, it can be seen that the z time series represents the transition between the excited SP and silent QS and exhibits periodicity.

As shown in Fig. 9, the ω-z plane conversion phase diagram is selected, the E point is selected as the starting point of the system motion track, and a stable limit ring appears in the direction given by arrow A, so the system has a small oscillation and is in an excited state. The system converges to a silent state at point F and transitions from point F to point G, and the system again oscillates slightly until point H. For the transition from point H to point I, the system enters the third excited state, gradually converges in the direction of C to D, and transitions from point J to point E.

According to the switching characteristics of the

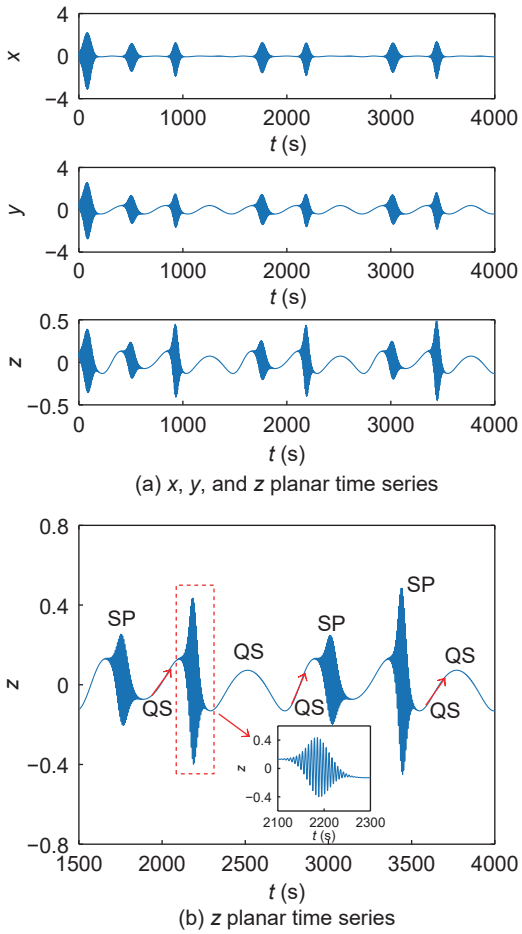

Fig. 8 Time series of state variables in the system.

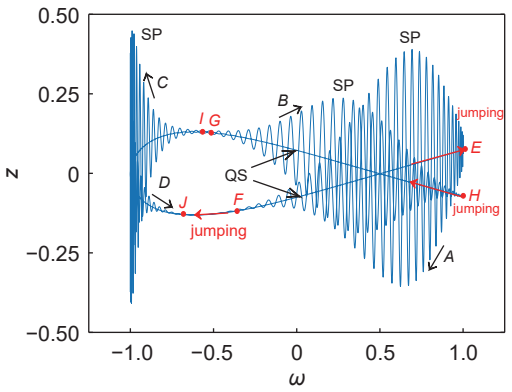

Fig. 9 ω-z plane conversion phase diagram.

memristor converter, the external joint excitation is added to working State 2 of the system, and by combining the equilibrium curve and the transition phase diagram of the fast on-cell system, it is found that the whole cycle cluster oscillation involves a three-Hopf bifurcation of the fast on-cell system, and the bistability of the equilibrium point of the stable limit ring is the key factor leading to the mutual transformation of the system rails between the silent

state and the excited state.

To verify the correctness of the above theoretical analysis, we used MATLAB/Simulink to build the circuit and verify the behavior of the system. Figure 10 shows the circuit model.

Figure 11 shows the time series plot of the three state variables of the system. We can see that Fig. 11 is in agreement with Fig. 8a, which verifies the correctness of the theoretical analysis.

5 Chaos Suppression for the Hybrid Control Strategy

5.1 Fractional-order mixed control method

Fractional-order three-dimensional chaotic system[32] is as follows:

$$\begin{cases} \dfrac{\mathrm{d}^{\alpha}x_1}{\mathrm{d}t^{\alpha}} = f_1(x_1,x_2,x_3,t), \\ \dfrac{\mathrm{d}^{\beta}x_2}{\mathrm{d}t^{\beta}} = f_2(x_1,x_2,x_3,t), \\ \dfrac{\mathrm{d}^{\gamma}x_3}{\mathrm{d}t^{\gamma}} = f_3(x_1,x_2,x_3,t) \end{cases} \tag{21}$$

where x_1, x_2, and x_3 represent the inductor current i_L, the capacitor voltage v_c, and the memristor capacitor voltage v_0, respectively.

The new state variables $\hat{x}_1$, $\hat{x}_2$, and $\hat{x}_3$ are introduced, and their relationship with x_1, x_2, and x_3 are expressed as follows:

$$\begin{cases} \hat{x}_1 = (1-s)x_1 + s(x_2+x_3), \\ \hat{x}_2 = (1-s)x_2 + s(x_1+x_3), \\ \hat{x}_3 = (1-s)x_3 + s(x_1+x_2) \end{cases} \tag{22}$$

The externally adjustable parameter s represents the strength of coupling between the state variables. The value range is 0–1, and $s(x_2+x_3)$, $s(x_1+x_3)$, and $s(x_1+x_2)$ represent the feedback of the system state. When s=0, there is no coupling relationship between the state variables. Replacing x_1, x_2, and x_3 in Eq. (21) with the new variables $\hat{x}_1$, $\hat{x}_2$, and $\hat{x}_3$ gives the following controllable system:

$$\begin{cases} \dfrac{\mathrm{d}^{\alpha}x_1}{\mathrm{d}t^{\alpha}} = f_1(\hat{x}_1,\hat{x}_2,\hat{x}_3,t), \\ \dfrac{\mathrm{d}^{\beta}x_2}{\mathrm{d}t^{\beta}} = f_2(\hat{x}_1,\hat{x}_2,\hat{x}_3,t), \\ \dfrac{\mathrm{d}^{\gamma}x_3}{\mathrm{d}t^{\gamma}} = f_3(\hat{x}_1,\hat{x}_2,\hat{x}_3,t) \end{cases} \tag{23}$$

Let $E_1(x_1,x_2,x_3)$ and $E_1(\hat{x}_1,\hat{x}_2,\hat{x}_3)$ be the correlation of the three state variables before and after the coupling of the fractional-order memristor load converter system, then:

$$\begin{aligned} &E_1(\hat{x}_1,\hat{x}_2,\hat{x}_3) = E_1\{[(1-s)x_1 + s(x_2+x_3)]\times \\ &[(1-s)x_2 + s(x_1+x_3)]\times[(1-s)x_3 + s(x_1+x_2)]\} = \\ &s^2(1-s)[x_1^3 + x_2^3 + x_3^3 + x_1^2(x_2+x_3) + x_2^2(x_1+x_3) + \\ &x_3^2(x_1+x_2) + 3x_1x_2x_3] + s(1-s)^2[x_1^2(x_2+x_3) + \\ &x_2^2(x_1+x_3) + x_3^2(x_1+x_2)] + (1-s)^3x_1x_2x_3 + \\ &s^3(x_1+x_2)(x_2+x_3)(x_1+x_3) \end{aligned} \tag{24}$$

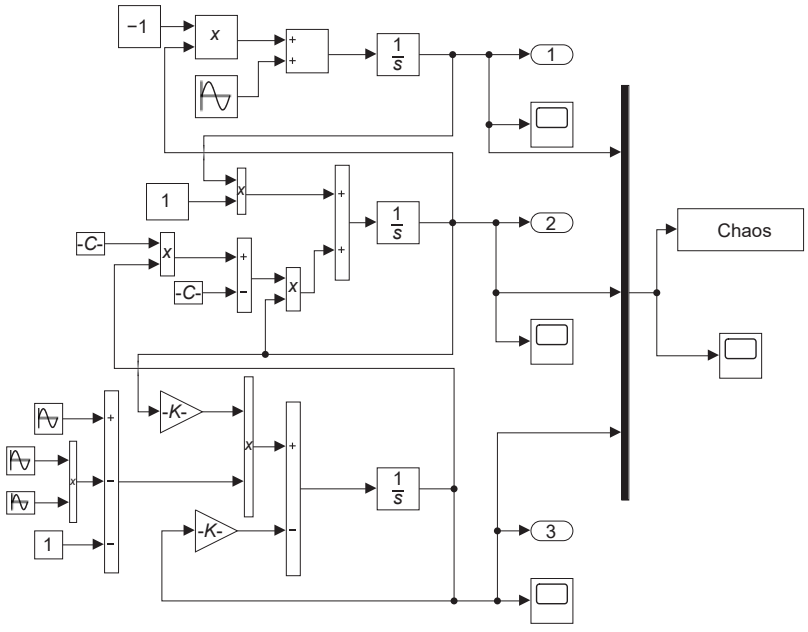

Fig. 10 Circuits simulated by Simulink.

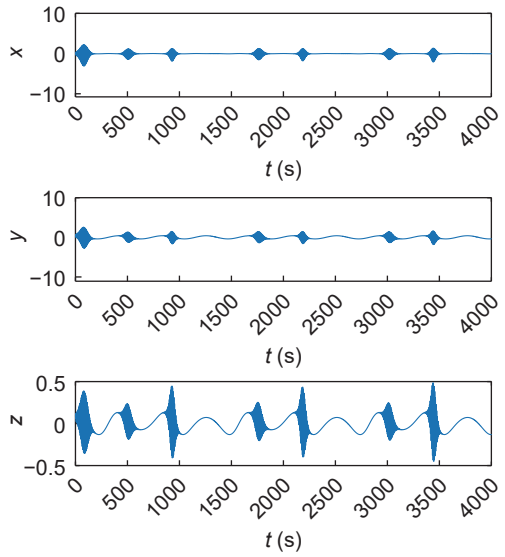

Fig. 11 Time series plot of state variables under Simulink.

According to the ternary fundamental inequality:

If $a,b,c\in\mathbb{R}$, then $a^3+b^3+c^3\geqslant 3abc$ if, and only if, $a=b=c$ is equal.

Thus,

$$s^2(1-s)(x_1^3+x_2^3+x_3^3)<3s^2(1-s)x_1x_2x_3, s<0 \tag{25}$$

From Eqs. (24) and (25), the following can be seen:

$$E_1(\hat{x}_1,\hat{x}_2,\hat{x}_3)<E_1(x_1,x_2,x_3), s<0 \tag{26}$$

Therefore, the coupling strength s has practical physical meaning.

5.2 Fractional-order Buck-Boost converter hybrid control design with memristor load

Design of a three-dimensional hybrid control system:

$$\begin{cases}\dfrac{\mathrm{d}^\alpha x_1}{\mathrm{d}t^\alpha}=\hat{f}_1(\hat{x}_1,\hat{x}_2,\hat{x}_3,t)=(1-s)f_1(\hat{x}_1,\hat{x}_2,\hat{x}_3,t)+\\ \qquad s[f_2(\hat{x}_1,\hat{x}_2,\hat{x}_3,t)+f_3(\hat{x}_1,\hat{x}_2,\hat{x}_3,t)],\\ \dfrac{\mathrm{d}^\beta x_2}{\mathrm{d}t^\beta}=\hat{f}_2(\hat{x}_1,\hat{x}_2,\hat{x}_3,t)=(1-s)f_2(\hat{x}_1,\hat{x}_2,\hat{x}_3,t)+\\ \qquad sf_3(\hat{x}_1,\hat{x}_2,\hat{x}_3,t),\\ \dfrac{\mathrm{d}^\gamma x_3}{\mathrm{d}t^\gamma}=\hat{f}_3(\hat{x}_1,\hat{x}_2,\hat{x}_3,t)=(1-s)f_3(\hat{x}_1,\hat{x}_2,\hat{x}_3,t)\end{cases} \tag{27}$$

From Eq. (27), Status 1:

$$\begin{aligned}\frac{\mathrm{d}^\alpha x_1}{\mathrm{d}t^\alpha}&=\hat{f}_1(\hat{x}_1,\hat{x}_2,\hat{x}_3,t)=\\ &(1-s)aE+s\{[cg\hat{x}_3-d]\hat{x}_2+[-m\hat{x}_2-p\hat{x}_3]\}=\\ &(1-s)aE+cgs(1-s)x_2^2+cgs^3x_1^2+\\ &cgs^2(2-s)x_1x_2+cgs^2x_2x_3+cgs^3x_1x_3-\\ &s^2(m+p)x_1+ms(1-s)x_2+ps(1-2s)x_2-ms^2x_3,\end{aligned}$$

$$\begin{aligned}\frac{\mathrm{d}^\beta x_2}{\mathrm{d}t^\beta}&=\hat{f}_2(\hat{x}_1,\hat{x}_2,\hat{x}_3,t)=\\ &(1-s)[cg\hat{x}_3-d]\hat{x}_2+s[-m\hat{x}_2-p\hat{x}_3]=\\ &cg(1-s)^3x_2x_3+cgs(1-s)^2(x_1x_3+x_3^2)-\\ &cgs(1-s)^2(x_1x_2+x_2^2)+cgs^2(1-s)(x_1+x_2)(x_1+x_3)-\\ &[d(1-s)+ms][(1-s)x_2+s(x_1+x_3)]-\\ &ps[(1-s)x_3+s(x_1+x_2)],\\ \frac{\mathrm{d}^\gamma x_3}{\mathrm{d}t^\gamma}&=\hat{f}_3(\hat{x}_1,\hat{x}_2,\hat{x}_3,t)=(1-s)[-m\hat{x}_2-p\hat{x}_3]=\\ &(p-m)s(1-s)x_1+[ps[(1-s)-m(1-s)^2]x_2-\\ &[ms[(1-s)+p(1-s)^2]x_3\end{aligned} \tag{28}$$

Similarly, from Eq. (27), Status 2:

$$\begin{cases}\dfrac{\mathrm{d}^\alpha x_1}{\mathrm{d}t^\alpha}=\hat{f}_1(\hat{x}_1,\hat{x}_2,\hat{x}_3,t)=\\ \qquad -(1-s)a\hat{x}_2+s\{[b\hat{x}_1+(cg\hat{x}_3-d)\hat{x}_2]+(-m\hat{x}_2-p\hat{x}_3)\}=\\ \qquad -a(1-s)^2x_2-as(1-s)(x_1+x_3)+bs(1-s)x_1+\\ \qquad bs^2(x_2+x_3)-cgs(1-s)x_3-(cg+p)s^2(x_1+x_2)+\\ \qquad (d-m)s(1-s)x_2+(d-m)s^2(x_1+x_3)-ps(1-s)x_3,\\ \dfrac{\mathrm{d}^\beta x_2}{\mathrm{d}t^\beta}=\hat{f}_2(\hat{x}_1,\hat{x}_2,\hat{x}_3,t)=\\ \qquad (1-s)[b\hat{x}_1+(cg\hat{x}_3-d)\hat{x}_2]+s(-m\hat{x}_2-p\hat{x}_3)=\\ \qquad b(1-s)[(1-s)x_1+s(x_2+x_3)]+\\ \qquad cg(1-s)[(1-s)x_3+s(x_1+x_2)][(1-s)x_2+s(x_1+x_3)]-\\ \qquad d[(1-s)x_2+s(x_1+x_3)]-ms[(1-s)x_2+s(x_1+x_3)]-\\ \qquad ps[(1-s)x_3+s(x_1+x_2)],\\ \dfrac{\mathrm{d}^\gamma x_3}{\mathrm{d}t^\gamma}=\hat{f}_3(\hat{x}_1,\hat{x}_2,\hat{x}_3,t)=\\ \qquad (1-s)(-m\hat{x}_2-p\hat{x}_3)=\\ \qquad (p-m)s(1-s)x_1+\\ \qquad [ps(1-s)-m(1-s)^2]x_2-[ms(1-s)+p(1-s)^2]x_3\end{cases} \tag{29}$$

6 System Simulation and Result Analysis

Based on the three-dimensional equation of state where the mixing control is applied, the following parameter values are selected: $E=2$ V, $a=b=c=g=1$, $d=0.2$, $m=0.25$, and $p=0.96$. These values are instituted to design the control effect of the control strategy.

Figure 12 shows a bifurcation plot of the inductor voltage of the converter as a function of the coupling strength s after hybrid control of the whole, fractional-order and memristor load, and resistive load converter.

From Fig. 12a, it can be seen that the external adjustable coupling control parameter s of the memristor system has different ranges of stability for the controlled system at orders 0.9 and 1.0. When the

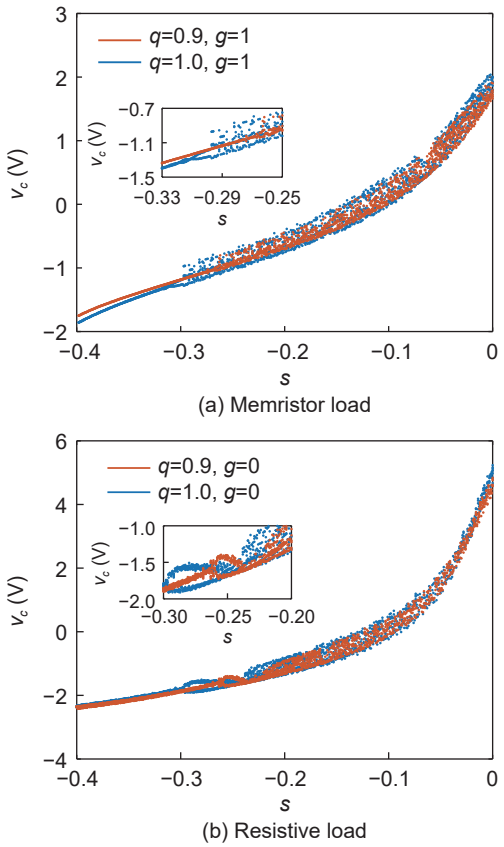

Fig. 12 Bifurcation diagram of control applied.

order of the system is 0.9, s controls the stability of the chaotic state of the system in the interval of [–0.4, –0.29]. Furthermore, s stabilizes the system in the range [–0.29, –0.26]. When the order of the system is 1.0, s stabilizes the chaotic state of the system in the interval of [–0.4, –0.33] to the periodic state, and s stabilizes the system in the interval of [–0.33, –0.28] to a double-cycle state. Comprehensively comparing the control performance of the 0.9-order and integer-order, the fractional-order system has a wider stabilizing cycle-one operating region, which further shows that the fractional-order system is more accurate than the integer-order system.

Similar to Fig. 12a, the system with a purely resistive load shown in Fig. 12b has different ranges of stability for 1.0 and 0.9 order of the system under the control of the external adjustable coupling control parameter s. When the order of the system is 0.9, s controls the stability of the chaotic state of the system in the interval of [–0.4, –0.26] in the periodic state, and s stabilizes the system in the interval [–0.26, –0.24] to the double-cycle state. When the order of the system is 1.0, s stabilizes the chaotic state of the system in the interval of [–0.4, –0.3] to the periodic state, and s stabilizes the system in the range [–0.3, –0.24]. Comprehensively comparing the stabilization range of the 0.9-order and 1.0-order control systems, the fractional-order system is stabilized over a wider range of period one operation, which reveals the dynamics of the system more accurately.

To investigate the effect of memristive and purely resistive loads on the stability intervals of the system, we select a fractional-order system for analysis. Comparing the orange fractional-order bifurcation curves in Fig. 12, it can be seen that the memristive load curve is more stable than the purely resistive load curve in the period one range and has the effect of expanding the stability range by a small margin.

As can be seen from Fig. 13, the controlled Lyapunov index indicates that the system is in a steady state when the index is less than zero and that the system is in a chaotic state when the index is greater than zero. A comprehensive comparison of the integer and fractional Lyapunov exponent (LE) curves of Fig. 13 shows that when the order is 0.9, the system has higher accuracy than the integer-order, and the control effect is more stable. Regardless of the resistive load or

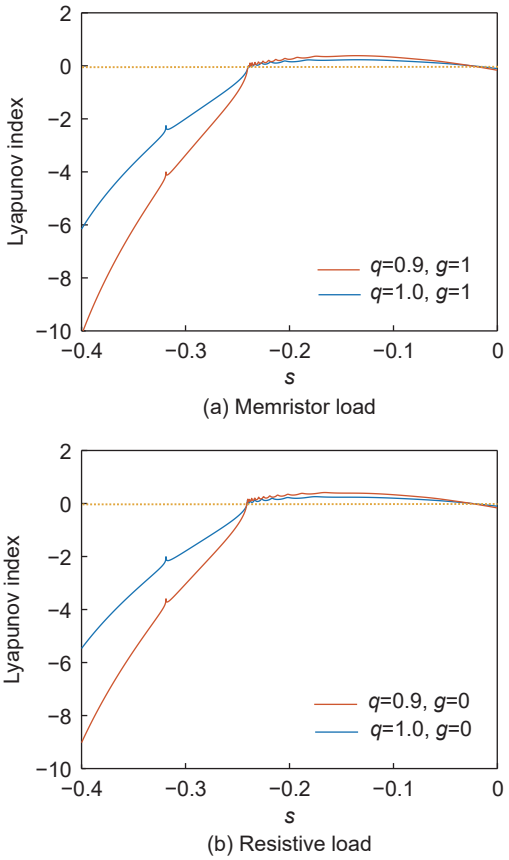

Fig. 13 Applying control LE diagram.

memory load of the system, the designed three-dimensional hybrid control strategy can control the system chaos phenomenon in a stable periodic state.

When the following parameters are chosen for the fractional Buck-Boost converter with a memristor load, the system exhibits chaotic properties. Its nonlinear properties gradually decrease with the coupling strength s in the range of interval [–0.4, 0], so the system is controlled in a stable periodic state.

Figures 14a–14c are time series plots of the three-state variables inductor current i_L, capacitor voltage v_c, and memristor capacitor voltage v_0 of the 0.9 order converter controlled at period 1 when $s = -0.4$, respectively. Figure 14d shows the system phase diagram of the two state variables of the inductor current and capacitor voltage, which has a closed and irregular periodic orbit when the inductor current i_L is not zero over time, that is, when the circuit operates in CCM mode.

Figure 15 shows the time domain curve and phase diagram of each state variable when the system order is 0.9 and the externally adjustable parameter $s = -0.285$. As can be seen from the diagram, the system is steered from the original chaotic state to a stable multiperiodic state.

Figure 16 shows the time domain curve and phase diagram of each state variable when the system order is 0.9 and the external tunable parameter $s = -0.1$. In the time domain waveform of the inductor current i_L, the length of time between two adjacent minimums is a switching cycle, and the switching period (or duty cycle) changes are chaotic. As can be seen from Fig. 16,

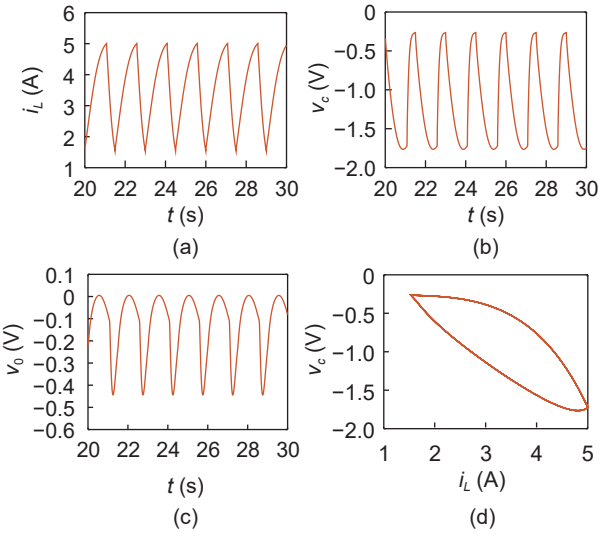

Fig. 14 Time domain curve and phase diagram of each state variable ($s = -0.4$ and $q = 0.9$, Cycle 1 state).

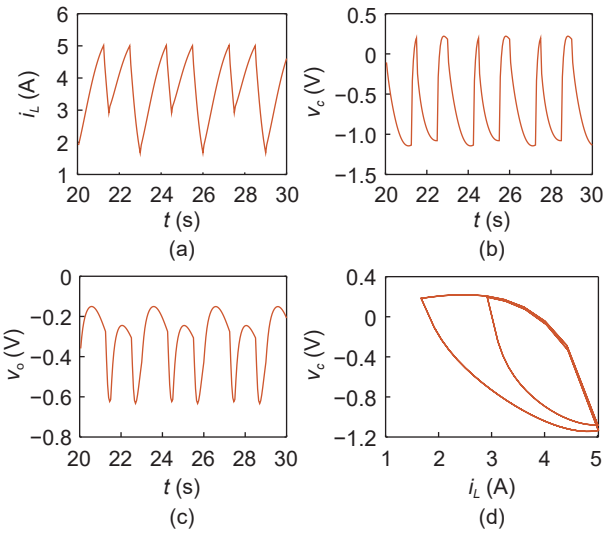

Fig. 15 Time domain curve and phase diagram of each state variable ($s = -0.285$ and $q = 0.9$, Cycle 2 state).

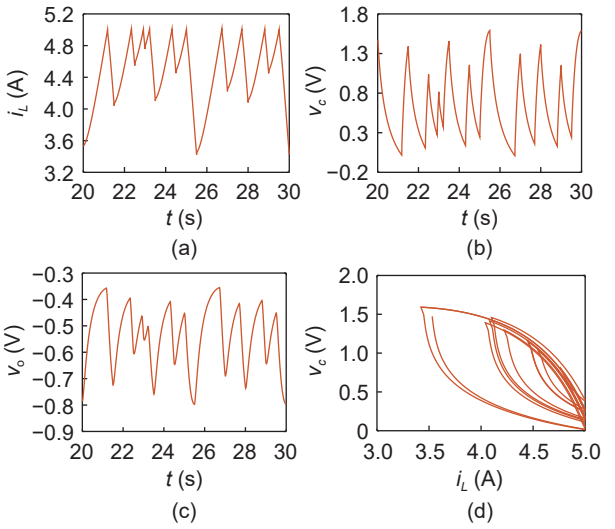

Fig. 16 Time domain curve and phase diagram of each state variable ($s = -0.1$ and $q = 0.9$, chaotic state).

the system is in a chaotic state.

Similar with the fractional-order control, integer-order systems can achieve stability control of each state variable separately for a certain control strength s. Figure 17 shows the time domain curve and phase diagram of each state variable when the system order is 1 and the external tunable parameter is $s = -0.38$. As can be seen from Fig. 17, the system is steered from the original chaotic state to a stable periodic state.

Figure 18 shows the time domain curve and phase diagram of each state variable when the system order is 1 and the external tunable parameter $s = -0.3$. It can be seen from Fig. 18 that when the control parameter s changes, the system motion changes from period T to period $2T$, its oscillation period doubles, and the system

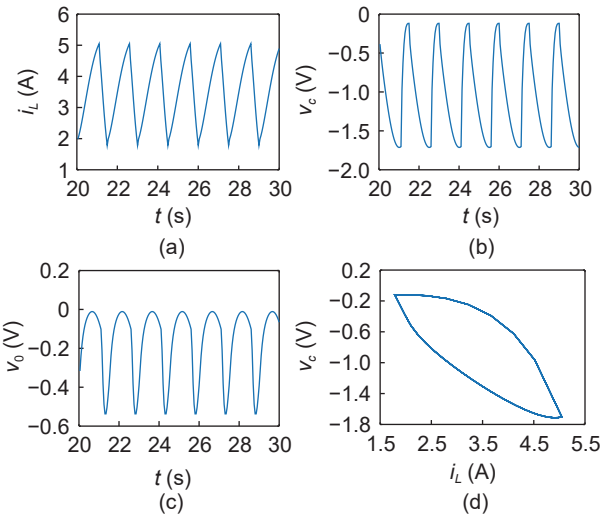

Fig. 17 Time domain curve and phase diagram of each state variable (s = −0.38 and q = 1.0, Cycle 1 state).

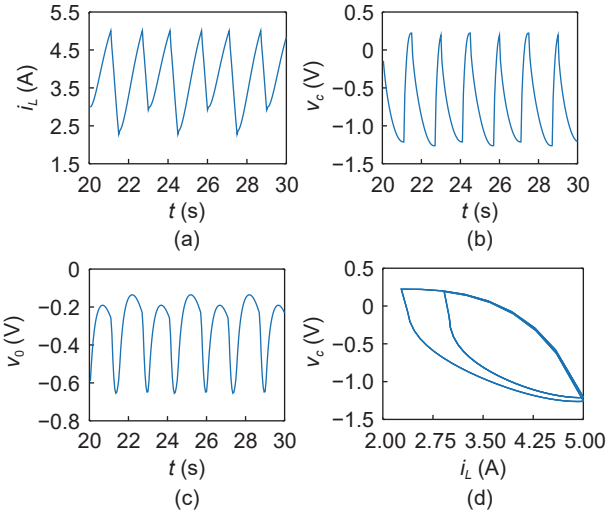

Fig. 18 Time domain curve and phase diagram of each state variable (s = −0.3 and q = 1.0, Cycle 2 state).

changes from the initial chaotic periodic state to the doubled period state.

Figure 19 shows the time domain curve and phase diagram of each state variable when the system order is 1.0 and the externally adjustable parameter s = −0.1. As can be seen from Fig. 19, the system is in a chaotic state. There are countless different periodic orbitals in the system, and its topology is transitive. As can be seen from Fig. 19d, when the circuit produces chaotic oscillations, the inductor current i_L is always greater than zero, and the circuit operates in CCM mode.

It can be seen from the above control results that for both the fractional and integer-order memristor load Buck-Boost converter, the method only needs to adjust an externally adjustable parameter s to control the

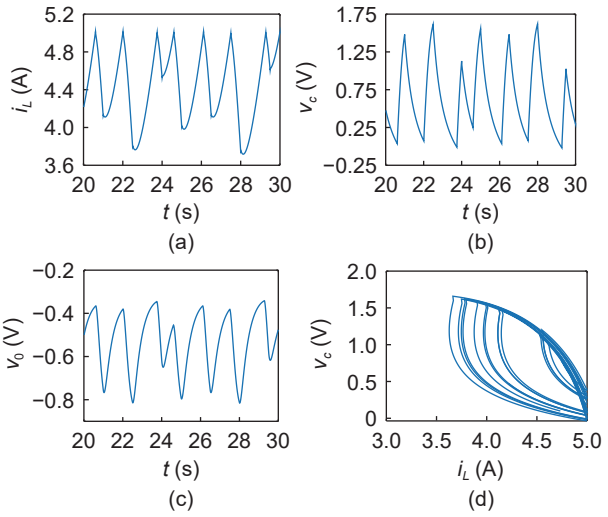

Fig. 19 Time domain curve and phase diagram of each state variable (s = −0.1 and q = 1.0, chaotic state).

Period 1, Cycle 2 track, and chaotic state of the converter in any state, which has the characteristics of a simple control structure, strong adaptability, and good control effect. This provides a new method for the chaotic control of the fractional-order memristor load converter.

7 Conclusion

In this study, a hybrid control strategy based on the fractional-order estimation-correction method is proposed to control the chaotic phenomenon of a three-dimensional fractional-order Buck-Boost converter operating in continuous mode with an inductor current in a stable periodic state. The following findings were revealed.

(1) According to the operating principle of the Buck-Boost converter, the one-cycle mathematical model of the system is established. The estimation-correction model has the advantages of accurate modeling, quick calculation, and no limitation from the sequence. Using the estimation coefficient, correction coefficient and initial value estimation expression, the accurate inductor current, and capacitor voltage of the fractional-order memristor load converter can be calculated directly to better analyze the dynamic characteristics of the fractional-order system.

(2) To verify the effectiveness of the designed chaos control method, first, by analyzing the bifurcation diagram, LE, and the Poincare cross-section of the system when the section x = −5 for certain parameters, it is verified that the system is in a chaotic state when the reference current is I_{ref} = 5 A. According to the

switching characteristics of the memristor converter, the external joint excitation is introduced to working State 2 for the system and combined with the time series and transition phase diagram of the fast subsystem. It is found that the system has a bursting oscillation phenomenon of three-Hopf bifurcation.

(3) Based on the idea of parameter perturbation and state association, a three-dimensional hybrid control strategy for the fractional-order memristor Buck-Boost converter is designed for which the control intensity is related only to the value of the external adjustable parameter s, which represents the coupling intensity between the state variables. It is demonstrated that at $s \in [-0.4, 0]$, as s decreases, the originally chaotic system can be controlled in a stable periodic state. Compared with fractional and integer-order control systems, the controlled system has a larger stability interval and a more accurate description of the physical properties of the system when the order is at 0.9 order.

This is further evidence of not only the rationality and workability of the estimation-correction method modeling but also the effectiveness of the three-dimensional mixture control developed. This method has a certain theoretical guiding value for the parameter optimization and controller design of the converter.

Acknowledgment

This work was supported by the Natural Science Foundation of Xinjiang Uygur Autonomous Region (Nos. 2022D01C367 and 2022D01E33) and National Natural Science Foundation of China (Nos. 52065064 and 52267010).

References

[1] M. B. Camara, H. Gualous, F. Gustin, A. Berthon, and B. Dakyo, DC/DC converter design for supercapacitor and battery power management in hybrid vehicle applications—Polynomial control strategy, *IEEE Trans. Ind. Electron.*, vol. 57, no. 2, pp. 587–597, 2010.

[2] N. Katayama, S. Tosaka, T. Yamanaka, M. Hayase, K. Dowaki, and S. Kogoshi, New topology for DC–DC converters used in fuel cell–electric double layer capacitor hybrid power source systems for mobile devices, *IEEE Trans. Ind. Applicat.*, vol. 52, no. 1, pp. 313–321, 2016.

[3] M. Zhioua, A. E. Aroudi, S. Belghith, J. M. Bosque-Moncusí, R. Giral, K. Al Hosani, and M. Al-Numay, Modeling, dynamics, bifurcation behavior and stability analysis of a DC–DC boost converter in photovoltaic systems, *Int. J. Bifurcation Chaos*, vol. 26, no. 10, p. 1650166, 2016.

[4] Z. Liao, Z. Liu, L. Chen, M. Lyu, Z. Wang, D. Wang, F. Wu, and H. Wei, An integrated observer framework based mechanical parameters identification for adaptive control of permanent magnet synchronous motor, *Complex System Modeling and Simulation*, vol. 2, no. 4, pp. 354–367, 2022.

[5] H. Zhang, S. Dong, W. Guan, C. Yi, and B. He, Adaptive control of fast-scale bifurcation in peak current controlled buck-boost inverter via one-cycle compensation, *Int. J. Bifurcation Chaos*, vol. 26, no. 12, p. 1650201, 2016.

[6] N. N. Yang, C. X. Liu, and C. J. Wu, Modeling and dynamics analysis of the fractional-order Buck-Boost converter in continuous conduction mode, *Chin. Phys. B*, vol. 21, no. 8, p. 080503, 2012.

[7] Z. Yao and L. Cai, Single-stage buck-boost off-grid inverter with feedforward control, *Int. J. Circuit Theory Appl.*, vol. 51, no. 6, pp. 2705–2715, 2023.

[8] B. Zhu, Q. Fan, G. Li, and D. Wang, Chaos suppression for a Buck converter with the memristive load, *Analog Integr. Circuits Signal Process.*, vol. 107, no. 2, pp. 309–318, 2021.

[9] J. Zhang, Y. Yang, and D. Wang, Dynamic analysis and chaos control of the switched-inductor boost converter with the memristive load, *Int. J. Circuit Theory Appl.*, vol. 49, no. 7, pp. 2007–2020, 2021.

[10] R. Zhang, A. Wu, Z. Wang, and S. Cang, Chaotic and subharmonic oscillations in a DC–DC boost converter with PWM voltage–current hybrid controller and parallel MR load, *Nonlinear Dyn.*, vol. 99, no. 2, pp. 1321–1339, 2020.

[11] L. Q. Zheng and Y. Peng, Chaos control of voltage mode controlled buck-boost converter, *Acta Phys. Sin.*, vol. 65, no. 22, p. 220502, 2016.

[12] L. Wang, X. Ni, Y. Hu, and R. Zhang, Chaos control of bi-directional DC-DC converter by resonant parametric perturbation method in a DC microgrid, *J. Phys.*: *Conf. Ser.*, vol. 1187, no. 2, p. 022033, 2019.

[13] J. Zhang, S. Li, C. K. Ahn, and Z. Xiang, Sampled-data output voltage regulation for a DC–DC buck converter nonlinear system with actuator and sensor failures, *Nonlinear Dyn.*, vol. 99, no. 2, pp. 1243–1252, 2020.

[14] D. N. Hajian, J. Ramadoss, H. Natiq, F. Parastesh, K. Rajagopal, and S. Jafari, Dynamics of Hindmarsh–Rose neurons connected via adaptive memristive synapse, *Chin. J. Phys.*, vol. 87, pp. 311–329, 2024.

[15] M. Ma, K. Xiong, Z. Li, and Y. Sun, Dynamic behavior analysis and synchronization of memristor-coupled heterogeneous discrete neural networks, *Mathematics*, vol. 11, no. 2, p. 375, 2023.

[16] B. Bao, X. Zhang, H. Bao, P. Wu, Z. Wu, and M. Chen, Dynamical effects of memristive load on peak current mode buck-boost switching converter, *Chaos Solitons Fractals*, vol. 122, pp. 69–79, 2019.

[17] C. Wu, Q. Zhang, N. Yang, R. Jia, and C. Liu, Dynamical analysis of a fractional-order boost converter with fractional-order memristive load, *Int. J. Bifurcation Chaos*, vol. 32, no. 3, p. 2250032, 2022.

[18] Y. Yang, D. Li, and D. Wang, Dynamic analysis of the switched-inductor buck-boost converter based on the memristor, *Electronics*, vol. 10, no. 4, p. 452, 2021.

[19] Y. Yu, M. Shi, H. Kang, M. Chen, and B. Bao, Hidden dynamics in a fractional-order memristive Hindmarsh–Rose model, *Nonlinear Dyn.*, vol. 100, no. 1, pp. 891–906, 2020.
[20] C. Wu, G. Si, Y. Zhang, and N. Yang, The fractional-order state-space averaging modeling of the Buck–Boost DC/DC converter in discontinuous conduction mode and the performance analysis, *Nonlinear Dyn.*, vol. 79, no. 1, pp. 689–703, 2015.
[21] Z. Yang, L. Bi, W. Chi, H. Shi, and C. Guan, Brain-controlled multi-robot at servo-control level based on nonlinear model predictive control, *Complex System Modeling and Simulation*, vol. 2, no. 4, pp. 307–321, 2022.
[22] B. Zhang, F. Xie, and R. Yang, Study on border collision and bifurcation of two-dimensional piecewise smooth systems in current mode controlled Buck converter, *Acta Phys. Sin.*, vol. 59, no. 12, pp. 8393–8407, 2010.
[23] C. Yang, F. Xie, Y. Chen, W. Xiao, and B. Zhang, Modeling and analysis of the fractional-order flyback converter in continuous conduction mode by caputo fractional calculus, *Electronics*, vol. 9, no. 9, p. 1544, 2020.
[24] L. Xie, Y. Yang, and J. Yao, Period doubling bifurcation of fractional order Boost converter based on predictor-corrector algorithm, *J. Power Supply*, pp. 1–14, 2023.
[25] L. Xie, J. Shi, J. Yao, and D. Wan, Research on the period-doubling bifurcation of fractional-order DCM Buck–Boost converter based on predictor-corrector algorithm, *Mathematics*, vol. 10, no. 12, p. 1993, 2022.
[26] B. Yan, S. Wang, and S. He, Complex dynamics and hard limiter control of a fractional-order buck-boost system, *Math. Probl. Eng.*, vol. 2021, p. 5572840, 2021.
[27] L. Xie, Z. Liu, K. Ning, and R. Qin, Fractional-order adaptive sliding mode control for fractional-order buck-boost converters, *J. Electr. Eng. Technol.*, vol. 17, no. 3, pp. 1693–1704, 2022.
[28] M. Mohadeszadeh, N. Pariz, and M. R. Ramezani-al, A fractional reset control scheme for a DC-DC buck converter, *Int. J. Dyn. Contr.*, vol. 10, no. 6, pp. 2139–2150, 2022.
[29] K. Oldham and J. Spanier, The fractional calculus, *Math. Gazette*, vol. 56, pp. 396–400, 1974.
[30] X. Zhou, Dynamic analysis of a current DC-DC converter with memristor load, MS dissertation, School of Automation and Electronic Information, Xiangtan University, Xiangtan, China, 2021.
[31] S. Westerlund and L. Ekstam, Capacitor theory, *IEEE Trans. Dielect. Electr. Insul.*, vol. 1, no. 5, pp. 826–839, 1994.
[32] F. Y. Zhang, W. Hu, X. B. Chen, H. Chen, and X. M. Tang, Chaos control and anti-control in Boost converter based on altering correlation, *Acta Phys. Sin.*, vol. 64, no. 4, p. 048401, 2015.

Lin Wang is currently pursuing the MS degree in electronic information at Xinjiang University, Urumqi, China. Her research interest is nonlinear dynamics of power systems.

Hongli Zhang is a professor and doctoral supervisor at the School of Electrical Engineering, Xinjiang University, Urumqi, China, and a secretary at the School of Intelligent Science and Technology, Xinjiang University, Urumqi, China. His main research interests are nonlinear system dynamics, industrial system fault diagnosis, advanced control, machine learning, and swarm intelligence optimization.

Shaohua Zhang received the BS and MS degrees from Xinjiang University, Urumqi, China in 2018 and 2021, respectively. He is currently pursuing the PhD degree at the School of Electrical Engineering, Xinjiang University, Urumqi, China. His research interests include memristive neuron systems and circuits, discrete memristor maps, and design and implementation of brain-like neural circuits based on memristor.

Cong Wang is an associate professor and doctoral supervisor at the Department of Automation, School of Electrical Engineering, Xinjiang University, Urumqi, China. Her main research interests include nonlinear dynamic analysis and control of power system, wind speed and wind power prediction, integrated energy system, intelligent optimization and scheduling, and application of swarm intelligent optimization algorithm.

Ping Ma is an associate professor and doctoral supervisor at the Department of Automation, School of Electrical Engineering, Xinjiang University, Urumqi, China. Her main research interests include system dynamic modeling and signal processing, industrial artificial intelligence, fault diagnosis, life prediction, machine vision, health monitoring, and maintenance decision-making.